JOURNAL OF MATERIALS SCIENCE 26 (1991) 5488–5494

Axi-symmetric compression of solid cylinders

Part II *Rapid loading conditions*

A. P. SINGH‡, K. A. PADMANABHAN
Department of Metallurgical Engineering, Indian Institute of Technology, Madras 600 036, India

Cylinders of EN 24 steel and commercial aluminium were compressed at 0.2 and 10.0 s^{-1} (rapid loading conditions). The temperature rise due to plastic deformation increased with strain rate and was significantly more in steel than in aluminium. The shape of the observed true stress–true strain curves was similar to the temperature rise–true strain plots. In steel, beyond a certain strain, the flow stress decreased with increasing strain, but in aluminium, a direct relation between the observed true stress and the true strain existed over the entire deformation range. Under rapid loading conditions the ring compression test was more reliable than the Cook and Larke method. In both materials, in specimens of constant diameter up to a true strain of 30%–40%, the compressive yield stress, σ_0, was proportional to $H^{1/8}$, where H is the instantaneous height of the specimen. Beyond this strain level, σ_0 increased with the diameter-to-height ratio (as seen during slow loading). The various factors that can influence the shape of the observed true stress–true strain curves have been considered. Semi-empirical equations have been developed which ensured that the friction-corrected data covering four to five decades of strain rate superimposed fairly well, following suitable temperature or temperature and strain-rate corrections.

1. Introduction

Rapid loading improves the strength properties of materials and the rate of processing [1]. By dividing the input mechanical energy by the mechanical equivalent of heat, J^*, a rough estimate of the heat generated by plastic deformation is obtained [2].

Nearly isothermal conditions prevail at slow strain rates (Part I [3]). At higher strain rates, there is a temperature rise in the test specimen, because the rate of heat loss to the surroundings is slower than the rate of heat generation by plastic working. At very high strain rates, adiabatic conditions are approached.

Non-uniform temperature rise and microstructural variations in specimens arise from inhomogeneous strain and strain-rate gradients which also lead to a change in the shape of the stress–strain curve [4].

Strain localization in plane strain compression is analysed using slip line theory and the temperature rise here is measured using heat-sensitive films [5–11]. In plane strain compression under rapid loading conditions [9] the observed flow stress, σ_{obs}, decreased with increasing width-to-height ratio of the specimen up to a certain strain. Beyond this strain level, however, there was a direct dependence between the two variables (as seen in Part I [3]). The former observation is not easy to explain, but is of practical significance while reducing large sections.

A number of authors have considered the effects of stress, strain and temperature rise. There is some evidence that the temperature rise due to deformation is responsible for the dependence of the stress–strain curve on the specimen geometry [12–32]. Unambiguous results, however, are lacking.

In the present study, EN 24 steel and aluminium cylinders of different initial diameter, D_0, to height, H_0 ratios, D_0/H_0, were compressed at room temperature under rapid loading conditions. The temperature rise at the centre of the specimen was recorded throughout the deformation. The coefficient of friction, μ, was determined by a ring compression test and the Cook and Larke method when applicable, i.e. in the range where $\sigma_{obs} \propto (D/H)$ ratio, where D and H are the instantaneous diameter and height, respectively. Ring compression testing was shown to be more accurate.

Using the values of μ obtained from this test, the compressive yield stress–true strain curves were derived. Semi-empirical, temperature and strain-rate corrections were made so that the present curves could be superimposed on the data presented in Part I [3]. A similar study on two superplastic alloys [33] will be reported elsewhere.

2. Experimental procedure

EN 24 steel, received as a rod of diameter 25.40 mm, had the composition (wt %) C 0.34, Mn 0.49, Cr 0.92, Ni 1.80, S 0.01, P 0.02 and Fe balance. Cylindrical specimens of a constant diameter of 20.00 mm and

‡ *Present address*: Research and Development Centre for Iron and Steel, Steel Authority of India Limited, Ranchi 834 002, India.

0022–2461/91 $03.00 + .12 © *1991 Chapman & Hall*

different D_0/H_0 ratios of 1.00, 0.80 and 0.67 were machined from the rod. The smaller diameter used in this case (compared with Al, see below) ensured that the capacity of 100 tonne available on the hydraulic press was not exceeded.

A slab of aluminium of composition (wt %) Fe 0.18, Si 0.12, Al balance, was melted in a crucible furnace and cast into rods of 50.80 mm diameter. The bars were forged at room temperature to a diameter slightly greater than 25.40 mm. Cylindrical specimens of a constant diameter of 25.40 mm and different D_0/H_0 ratios of 1.00, 0.80 and 0.67 were machined from the forged rods.

From both the as-received EN 24 steel and forged Al rods, ring compression test specimens of dimensions 19.05 mm o.d. 9.50 mm i.d. and 6.35 mm height, H, were machined.

The two-dimensional grain size of EN 24 steel, in the as-received condition, was 10 ± 0.4 μm. The Al specimens were annealed at 673 K for 3.6 ks to obtain a two-dimensional grain size of 73 ± 0.2 μm.

The specimens were compressed on a 100 tonne hydraulic press at a mean strain rate of $0.2\,s^{-1}$ and on a 180 tonne friction screw press at a mean strain rate of $10.0\,s^{-1}$. The reduction in height was by about 70%.

The load, ram travel and temperature rise during deformation were recorded using an 'Oscillomat', which comprises an oscilloscope and a recording camera. The small mirrors attached to the mechanism perform oscillations that are proportional to the electrical variations of the deformation phenomenon. By means of an illuminating and imaging optical system, the mirror throws a small light spot on the recording paper. The X (width) directed movement of the spot traces a curve on the moving recording paper (Y direction). The recording paper is then chemically developed to obtain the traces.

Ram travel was recorded using a linear variable differential transducer (LVDT). The load measurements were made using a standard electrical resistance strain gauge dynamometer. For recording temperature rise during deformation, a coaxial chromel–alumel thermocouple of 1 mm o.d. was used. The thermocouple was inserted into a 1 mm hole made up to the axis of the cylinder at mid-height. Thus, the temperature rise at the centre of the specimen, which should correspond to the maximum value, could be recorded.

Ring compression tests were also done on the hydraulic and friction screw presses. The amount of compression varied between 10% and 50%.

The load–displacement curves were converted into observed true stress, σ_{obs}–true strain ε_t, plots. Maximum temperature rise, ΔT_{max},–true strain, ε_t, curves were derived from the maximum temperature rise–ram travel traces.

From the ring compression tests, the percentage change in the i.d. of the ring-percentage reduction in height curves was plotted for both materials.

After applying suitable temperature corrections (and, in the case of aluminium, a strain-rate correction as well), the results were compared with those pertaining to slow loading conditions (Part I [3]).

3. Results

At either strain rate, in both materials up to about 30%–40% true strain the taller specimens had a greater flow stress than the shorter ones (anomalous behaviour). But, beyond this strain, up to the maximum level (~ 70%) the converse was true; Fig. 1a and b for EN 24 steel; Fig. 1c and d for aluminium.

As the deformation was accompanied by a rise in temperature, the maximum temperature rise at the centre of the specimen, $(\Delta T)_{max}$, was recorded for each test; Fig. 2a and b correspond to steel and Fig. 2c to aluminium.

The results of a ring compression test on EN 24 steel are shown in Fig. 3, as an example. For this test, with steel specimens, both strain rates were used. But in aluminium the flow resistance and the specimen dimensions were too small for successful testing at a mean strain rate of $10.0\,s^{-1}$.

By comparison with standard charts (see Part I [3]) the coefficient of friction, μ, for steel at both strain rates was seen to be 0.15. For aluminium μ also equalled 0.15 at a strain rate of $0.2\,s^{-1}$. (In the subsequent calculations, the same value was also used for a strain rate of $10.0\,s^{-1}$.)

In its range of applicability, the Cook and Larke method gave values of 0.24 and 0.26 for μ in steel at strain rates of 0.2 and $10.0\,s^{-1}$, respectively. The corresponding value for aluminium at both strain rates was 0.18.

4. Discussion

Owing to greater work of deformation (much higher flow stress) and lower (by nearly a factor of 4) thermal conductivity (i.e. greater heat production and less loss), the temperature rise was considerably greater in steel than in aluminium. In both materials, the σ_{obs}–ε_t curves (Fig. 1a–d), as well as the $(\Delta T)_{max}$–ε_t plots (Fig. 2a–c), the different D_0/H_0 ratios crossed over at a true strain of about 30%–40%. This observation suggested that the shape of a σ_{obs}–ε_t curve was mainly influenced by the temperature rise in a test. In either material, before the cross-over in the flow curves, the flow stress decreased with increasing D/H ratio (anomalous behaviour) and this could be traced to the increase in the $(\Delta T)_{max}$ value with increasing D/H ratio. However, beyond the strain range at which the flow curves crossed over, σ_{obs} increased with the D/H ratio (conventional behaviour) as $(\Delta T)_{max}$ decreased with increasing D/H ratio. This result is attributed to the greater heat loss that results from an increase in the D/H ratio at large strain/time of deformation. (The surface area-to-volume ratio varies as $2\pi r(h + r)/\pi r^2 h$.) In other words, in the beginning the smaller heat capacity of a shorter specimen (larger D/H ratio) leads to a greater temperature rise, while above a certain strain the effects of heat loss to the surroundings become more important.

In steel the temperature rise was from about 140 °C (mean strain rate = $0.2\,s^{-1}$) to about 180 °C (mean strain rate = $10.0\,s^{-1}$). Therefore, at large strains thermal softening became more important than work

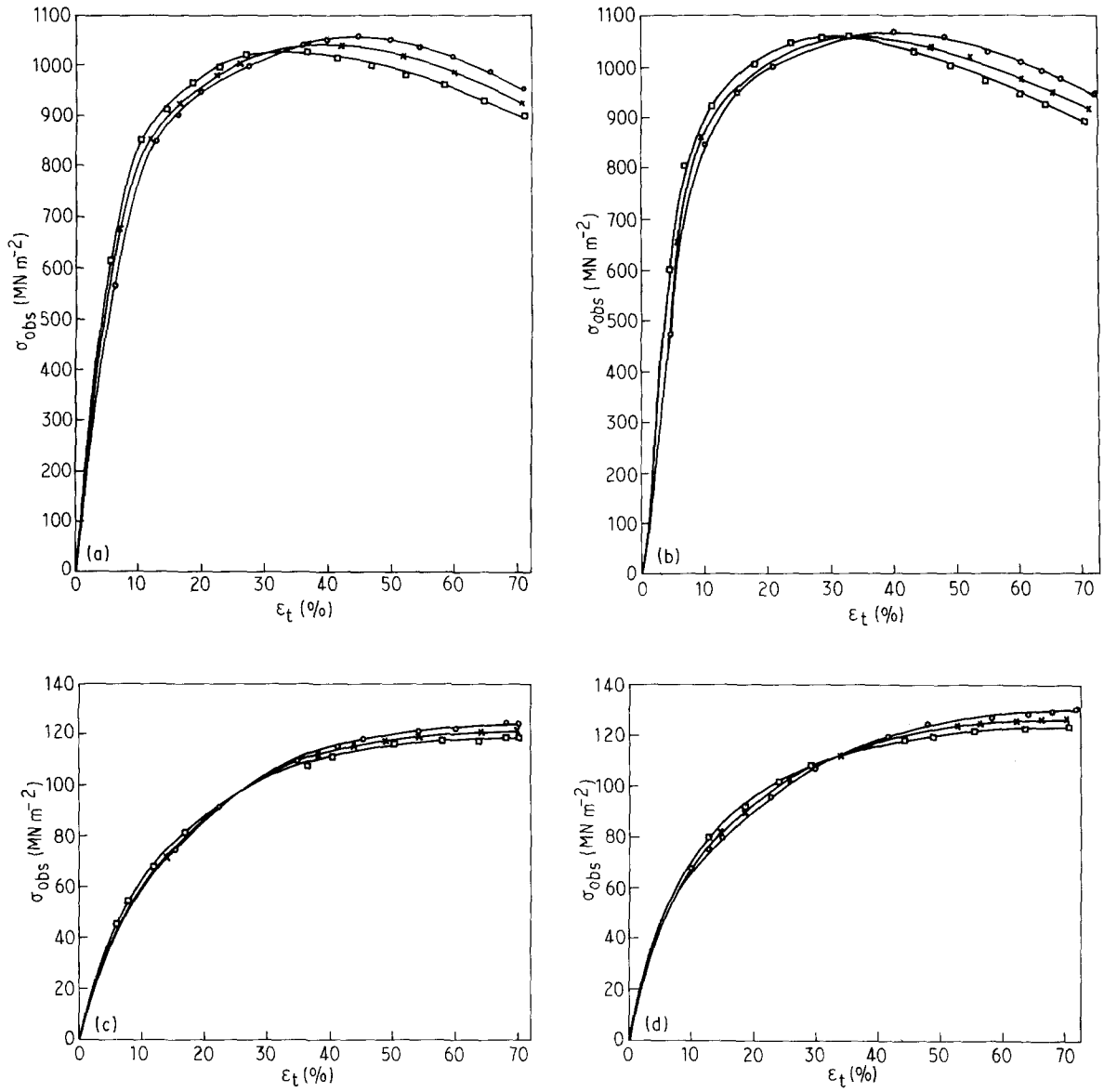

Figure 1 True compressive stress (including friction), σ_{obs},-per cent true strain, ε_t, relationship at room temperature for different initial diameter-to-height ratios, D_0/H_0: (○) 1.00, (×) 0.80, (□) 0.67. (a, b) EN 24 steel, grain size 10 μm. (c, d) Commercial aluminium, grain size 73 μm. Mean strain rate: (a, c) 0.2 s^{-1}, (b, d) 10.0 s^{-1}.

hardening and the flow stress decreased with increasing strain; Fig. 1a and b. In aluminium, on the other hand, temperature rise ranged only from less than 15 °C (mean strain rate = 0.2 s^{-1}) to less than 35 °C (mean strain rate = 10.0 s^{-1}), and so work hardening prevailed over thermal softening, i.e. the flow stress increased with strain over the entire deformation range (Fig. 1c, d).

For a Cook and Larke test to be valid, at a fixed strain the specimen temperature for all D/H ratios should be the same. This condition is not satisfied under the present experimental conditions (Fig. 2a–c). On the other hand, the ring compression test has been shown to be applicable over a wide range of strain rate and temperature. Therefore, μ obtained from ring compression testing was used to correct Fig. 1a–d for the presence of friction (using Equation 1 of Part I [3]). (While making these corrections, it is implicitly assumed that μ is constant throughout the deformation, and that it does not change with temperature in the range covered by room temperature to the highest temperature reached in the specimen as a result of plastic deformation. This approximation seems justified by the meaningful results that are obtained at the end of the calculations – see later.) The curves corrected for friction are given in Fig. 4a–d. In the initial portions of these curves, σ_0 (the compressive yield stress uncorrected for the temperature rise) was proportional to $H^{1/8}$, where H is the instantaneous height of the specimen.

An effort was made to superimpose the present results on the near-isothermal flow data obtained in Part I [3] by applying suitable temperature and (where necessary) strain-rate corrections. Then, material response over five decades of strain rate could be represented by appropriate equations. The assumption was made that at any given instant the average specimen temperature was proportional to T_{max} (= room temperature, $T_0 + (\Delta T)_{max}$), measured at that particular instant. The temperature dependence of the flow stress was assumed to be exponential and the increase in its magnitude due to heat lost to the

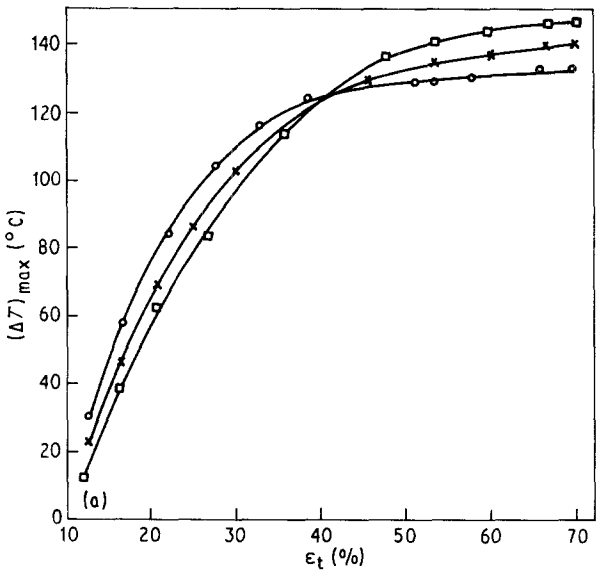

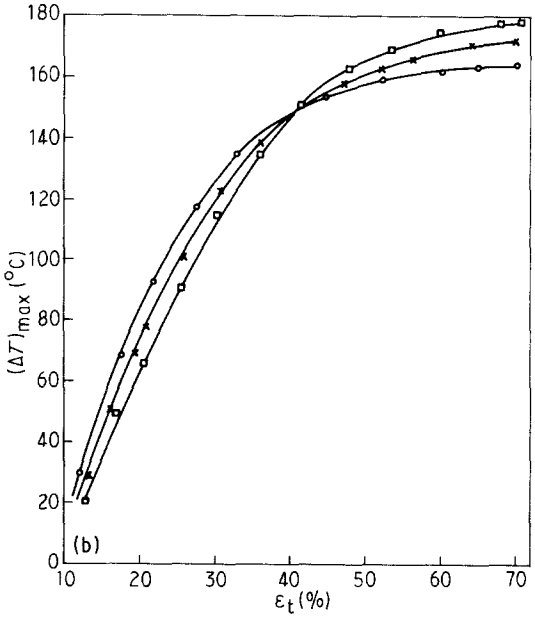

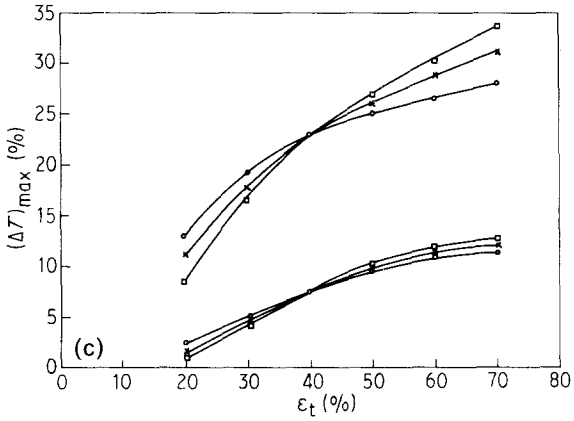

Figure 2 (Maximum) temperature rise at the centre of the specimen, $(\Delta T)_{max}$–ε_t relationship in room-temperature tests on specimens with different D_0/H_0 ratios (for key see Fig. 1). (a, b) EN 24 steel, grain size 10 μm. (c) Commercial aluminium, grain size 73 μm. Mean strain rate: (a) 0.2 s^{-1}, (b) 10.0 s^{-1}, (c) 0.2 s^{-1}, and 10.0 s^{-1}.

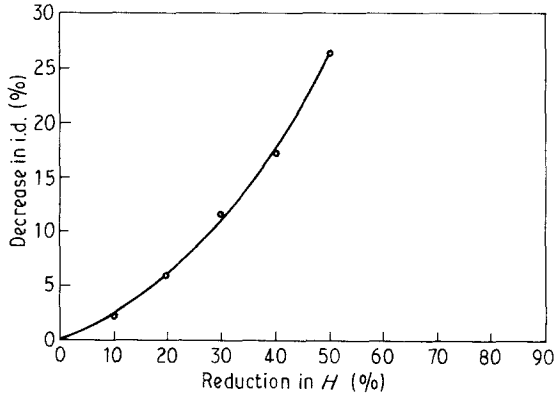

Figure 3 Percentage decrease in the internal diameter, i.d.–percentage reduction in height, H, relationship in a ring compression test at room temperature. EN 24 steel, grain size 10 μm, mean strain rate = 10.0 s^{-1}.

surroundings was included in the analysis through f(t), where f(t) is function of the time of deformation, t. That is

$$(\sigma_0)_d \propto \exp[(A_1/T_{max})f(t)] \quad (1)$$

where A_1 is a temperature-independent constant that incorporates an activation energy term, the gas constant and the constant of proportionality between T_{max} and the average specimen temperature. If $(\sigma_0)_s$ is the isothermal flow stress, then

$$(\sigma_0)_s \propto \exp(A_1/T_0) \quad (2)$$

Subscripts d and s represent, respectively, dynamic and slow loading conditions.

In the case of aluminium, the temperature rise was small. So the cooling effects due to heat lost to the surroundings could be neglected, i.e. f(t) = 1. Likewise, no strain-rate corrections were needed for steel, because of its very low strain-rate sensitivity of flow.

For aluminium, a mean strain-rate sensitivity index, m, of 0.05 was used in the strain-rate range 8.2×10^{-4} to 10.0 s^{-1} to allow for the effect of strain rate, i.e.

$$(\sigma_0^*)_d/(\sigma_0)_s \propto (\dot{\varepsilon}_d/\dot{\varepsilon}_s)^{0.05} \quad (3)$$

where $\dot{\varepsilon}_d$ and $\dot{\varepsilon}_s$ are, respectively, the strain rates under dynamic (rapid) and slow loading conditions. $(\sigma_0^*)_d$ is the flow stress at a strain rate in the rapid loading range, that is already corrected for the temperature rise.

Based on the above approach, the following quantitative relationships were established.

(i) EN 24 steel

$$\ln[(\sigma_0)_s/(\sigma_0)_d] = 19.30[\Delta T_{max}/\overline{T_0 T_{max}}]$$

$$\dot{\varepsilon}_{av} = 0.2\,s^{-1}, \quad \varepsilon_t < 30\%, \quad f(t) = 1, \quad (4)$$

$$\ln[(\sigma_0)_s/(\sigma_0)_d] = 19.30\exp(t)[\Delta T_{max}/\overline{T_0 T_{max}}]$$

$$\dot{\varepsilon}_{av} = 0.2\,s^{-1}, \quad 30\% < \varepsilon_t < 70\% \quad (5)$$

and

$$\ln[(\sigma_0)_s/(\sigma_0)_d] = 2.34 \times 10^5 (t)^{2.36}[\Delta T_{max}/\overline{T_0 T_{max}}]$$

$$\dot{\varepsilon}_{av} = 10.0\,s^{-1} \quad \text{for all strains.} \quad (6)$$

No strain-rate correction is necessary ($\dot{\varepsilon}_{av}$ = average strain rate).

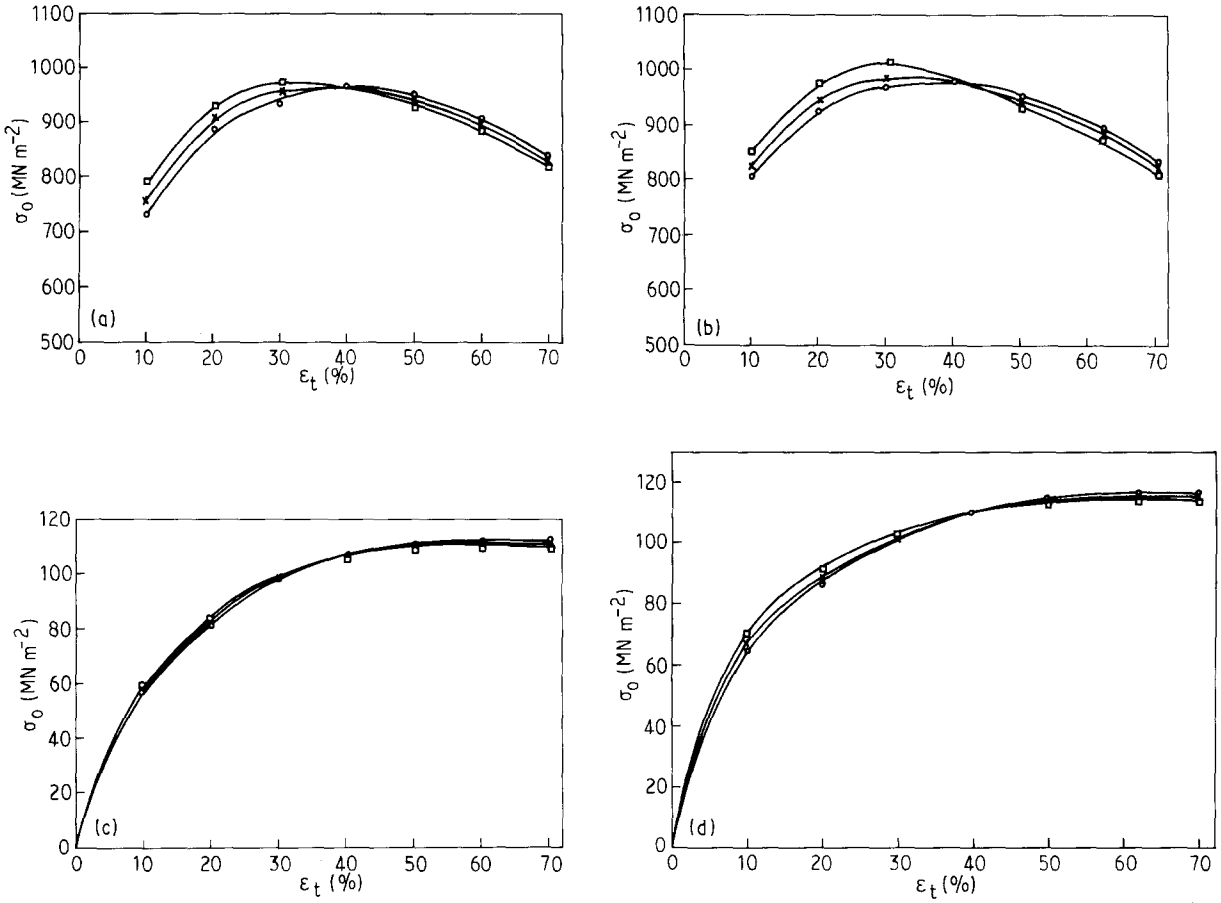

Figure 4 True compressive yield stress, σ_0,–ε_t relationship at room temperature for different D_0/H_0 ratios (for key, see Fig. 1). (a, b) EN 24 steel, grain size 10 μm. (c, d) Commercial aluminium, grain size 73 μm. Mean strain rate: (a, c) 0.2 s^{-1}, (b, d) 10.0 s^{-1}.

(ii) Aluminium

$$\ln[(\sigma_0^*)_d/(\sigma_0)_d] = 895\,[\Delta T_{max}/\overline{T_0\,T_{max}}]$$

$$\dot{\varepsilon}_{av} = 0.2\,s^{-1},\ f(t) = 1, \quad \text{for all strains,} \qquad (7)$$

and

$$\ln[(\sigma_0^*)_d/(\sigma_0)_d] = 698\,[\Delta T_{max}/\overline{T_0\,T_{max}}]$$

$$\dot{\varepsilon}_{av} = 10.0\,s^{-1},\ f(t) = 1, \text{ for all strains.} \qquad (8)$$

Subsequently a strain-rate correction is made using Equation 3.

The data corrected using Equations 4–6 in the case of EN 24 steel are given in Table Ia, along with results pertaining to the slow loading range. Evidently, data pertaining to the range 6×10^{-3} to 10.0 s^{-1} superimpose well.

Using Equations 7 or 8 and Equation 3, the data concerning aluminium are compared in Table Ib with results pertaining to a (slow) strain rate of 8.2×10^{-4} s^{-1}. Once again, the correlation between the slow loading and rapid loading test results is good. In a relative sense, however, the correlation is inferior for aluminium than for steel.

Thus, data spread over five decades of strain rate, involving ranges where a temperature rise was present as well as absent, could be well correlated using the present semi-empirical method. Alternative approaches based on the finite element or finite difference analysis are likely to be more involved.

Finally, equations similar to Equations 3–8 are useful in the choice of equipment as well as process optimization.

5. Conclusions

Based on the present experiments under rapid loading conditions, the following conclusions were drawn.

1. In both EN 24 steel and commerical aluminium the temperature rise due to plastic deformation increased with strain rate (because of reduced heat loss to the surroundings).

2. On account of the considerably greater work of deformation (arising from a much higher flow stress) and lower thermal conductivity (which leads to less heat losses), the temperature rise was significantly more in steel than in aluminium.

3. The shapes of the observed flow stress–true strain curves and the maximum temperature rise–true strain plots were similar. In steel, beyond a certain strain level the flow stress decreased with increasing strain. (The large temperature rise led to thermal softening.) As the temperature rise in aluminium was rather small, in the entire range the observed stress and strain were directly related.

4. The ring compression test was more reliable than the Cook and Larke technique for evaluating the coefficient of friction.

TABLE I Friction, temperature and strain-rate corrected flow stress at different true strains for specimens of different D_0/H_0 ratios deformed at various strain rates

(a) EN 24 steel

Strain rate (s^{-1})	D_0/H_0 ratio	Friction and temperature corrected flow stress ($MN\,m^{-2}$) at true strain (%) of					
		20	30	40	50	60	70
0.2	1.00	896	946	1045	1050	1050	1055
	0.80	915	965	1045	1050	1050	1050
	0.67	940	985	1045	1045	1050	1050
10.0	1.00	931	995	1045	1055	1060	1050
	0.80	956	1017	1045	1050	1050	1050
	0.67	981	1037	1045	1050	1045	1045
6.0×10^{-3} (see Part I: Table Ib)	Independent of D_0/H_0 ratio	932	975	1020	1035	1043	1048
Maximum error in prediction (static loading condition is used as the base):		5.3%	6.4%	2.5%	1.9%	1.6%	0.7%

(b) Commercial aluminium

Strain rate (s^{-1})	D_0/H_0 ratio	Friction, temperature and strain-rate corrected flow stress ($MN\,m^{-2}$) at true strain (%)					
		20	30	40	50	60	70
0.2	1.00	64.0	78.0	87.5	92.0	94.0	95.0
	0.80	64.5	79.0	88.5	93.0	95.0	96.0
	0.67	65.5	80.0	89.5	94.0	96.0	96.5
10.0	1.00	59.0	73.0	81.0	85.0	86.5	88.0
	0.80	60.3	73.3	81.7	85.8	87.3	89.0
	0.67	61.0	75.7	82.4	87.0	89.0	90.5
8.2×10^{-4} (see Part I: Table Ia)	Independent of D_0/H_0 ratio	72.5	79.5	84.0	87.0	89.0	91.5
Maximum error in prediction (static loading condition is used as the base):		18.6%	8.2%	6.5%	8.0%	7.9%	5.5%

5. In both EN 24 steel and commercial aluminium at both strain rates of 0.2 and $10.0\,s^{-1}$, up to a true strain of about 40% the (temperature uncompensated) true compressive yield stress was proportional to $H^{1/8}$, where H is the instantaneous height of the specimen.

6. The flow stress–true strain curves covering four to five decades of strain rate (extending from slow loading to rapid loading conditions) could be made to superimpose to a fair degree of accuracy, if (a) frictional contribution and temperature rise are accounted for in the case of EN 24 steel, and (b) corrections for frictional contribution, temperature rise and strain-rate changes are considered for aluminium. Equations 4–6 in the case of steel and Equations 7, 8 and 3 in the case of aluminium, facilitate the conversion of friction-corrected data pertaining to rapid loading conditions to slow loading conditions (and vice versa).

References

1. H. J. E. HAMEL, *J. South African Inst. Min. Met.* **72** (1972) 44.
2. G. E. DIETER, "Mechanical Metallurgy", 3rd Edn (McGraw-Hill International Student Edition, New York, 1986) pp. 524–6.
3. A. P. SINGH and K. A. PADMANABHAN, *J. Mater. Sci.* **26** (1991) 5481.
4. B. AHLBLOM and R. SANDSTRÖM, *Int. Met. Rev.* **27** (1982) 1.
5. R. HILL, "The Mathematical Theory of Plasticity" (Clarendon Press, Oxford, 1950) pp. 226–36, 254–8.
6. H. P. HEIL and A. SCHUTZA, *Arch. Eisenhüttenw.* **46** (1975) 201.
7. M. VATER and H. P. HEIL, *Stahl und Eisen* **91** (1975) 864.
8. C. H. LEE and S. KOBAYASHI, *Int. J. Mech. Sci.* **12** (1970) 949.
9. J. H. BEYNON and C. M. SELLARS, *J. Test. Eval.* **13** (1985) 28.
10. R. W. ARMSTRONG, C. S. COFFEY and W. L. ELBLAND, *Acta Metall.* **30** (1982) 2111.
11. A. K. SACHDEV and J. E. HUNTER, *Met. Trans.* **13A** (1982) 1063.
12. R. COLAS and C. M. SELLARS, *J. Test. Eval.* **15** (1987) 342.
13. W. LUEG, H. G. MÜLLER and V. KRAUSE, *Arch. Eisenhüttenw.* **28** (1957) 505.
14. J. A. BAILEY and A. R. E. SINGER, *J. Inst. Met.* **92** (1964–65) 288.
15. K. FINK, W. LUEG and G. BURGER, *Arch. Eisenhüttenw.* **26** (1955) 655.
16. J. B. HAWKYARD and T. B. POTTER, *Int. J. Mech. Sci.* **13** (1971) 171.
17. G. L. BARAYA, W. JOHNSON and R. A. C. SLATER, *Int. J. Mech. Sci.* **17** (1963) 621.
18. S. K. SAMANTHA, *ibid.* **10** (1968) 613.
19. J. L. CHIDDISTER and L. E. MALVERN, *Exp. Mech.* **3** (1963) 81.
20. A. C. WHIFFEN, *Proc. Roy. Soc. A* **194** (1948) 300.

21. J. F. BELL, "The Physics of Large Deformation of Crystalline Solids", 1st Edn (Springer Verlag, New York, 1968) p. 233.
22. H. KOLSKY and L. S. DOUGH, *J. Mech. Phys. Solids* **10** (1962) 141.
23. E. D. H. DAVIES and S. C. HUNTER, *ibid.* **11** (1963) 155.
24. U. S. LINDHOM, *ibid.* **12** (1964) 317.
25. S. K. SAMANTA, "Proceedings of the 11th International MTDR Conference", Birmingham (1970) p. 827.
26. J. R. DOUGLAS and T. ALTAN, *J. Eng. Ind. Trans. ASME* **47** (1975) 66.
27. C. E. N. STUGERS and A. N. BRAMLEY, "Proceedings of the 11th International MTDR Conference", Birmingham (1970) p. 803.
28. C. H. KARNES and E. A. RIPPERGER, *J. Mech. Phys. Solids* **14** (1966) 75.
29. U. S. LINDHOM and L. M. YEARKLEY, *ibid.* **13** (1965) 41.
30. J. B. HAWKYARD, D. EATON and W. JOHNSON, *Int. J. Mech. Sci.* **10** (1968) 929.
31. S. K. SAMANTHA, *ibid.* **11** (1969) 435.
32. J. F. ALDER and V. A. PHILLIPS, *J. Inst. Met.* **83** (1954–55) 80.
33. K. S. K. CHOCKALINGAM, PhD thesis, IIT Madras, India (1984).

Received 19 March
and accepted 20 December 1990